Tang T., Silva G. T., Huang L., & Han X. (2022). Acoustic levitation of axisymmetric Mie objects above transducer array by engineering the acoustic radiation force and torque. *Physical Review E* .
DOI: 10.1103/PhysRevE.106.045108

Acoustic levitation of axisymmetric Mie objects above transducer array by engineering the acoustic radiation force and torque

Tianquan Tang*
Department of Mechanical Engineering, The University of Hong Kong, Pokfulam, Hong Kong SAR, China

Glauber T. Silva
Physical Acoustics Group, Instituto de Física, Universidade Federal de Alagoas, Maceió, Alagoas, Brazil

Lixi Huang and Xue Han
Department of Mechanical Engineering, The University of Hong Kong, Pokfulam, Hong Kong SAR, China

Transducer arrays are a versatile tool for the contactless manipulation of spherical Rayleigh objects. Here, we propose an analytical model for stable levitation of axisymmetric Mie objects through directly engineering the desired radiation force and torque. Acoustic contributions from multiple transducers are superimposed through the translation addition theorem, and the non-spherical objects are mapped into a sphere using the conformal transformation technique so that the scattered field can be asymptotically obtained. Then, we give the acoustic radiation force and torque applied to a rigid non-spherical Mie object, which can be reconstructed as a series of quasi-explicit functions of the transducer (amplitude and phase) parameters. Through specifying the desired radiation force and torque exerted on the objects, a system of nonlinear equations is produced, which could be iteratively solved to retrieve appropriate transducer parameters that stabilize the object in an equilibrium position. Practically, we demonstrate several examples in stable levitation of a sphere, a spheroid, and a disk with an averaged radius of $a = 7$ mm (size parameter of $ka \approx 5.18$) above a transducer array. The absolute acoustic pressure field surrounding the objects simulated by the finite element method is illustrated to verify the trapping results. The developed analytical model provides an alternative approach to retrieve the transducer parameters for levitating macroscopic non-spherical rigid objects, which may help design the systematic dynamical manipulation of Mie particles.

I. INTRODUCTION

Time-averaged acoustic radiation force and torque on the levitated objects because of the momentum and angular momentum transfers that arises from acoustic scattering and absorbing effects of the wave-particle interaction have been derived from the integrations of Westervelt and Maidanik stresses [1–4]. Along this line, through the expression of stress tensors in the form of the partial wave expansion series, many works have established theoretical frameworks to evaluate the radiation force and torque exerted on a spherical particle in a viscous [5, 6] and an inviscid fluid [7–10]. The theoretical methods were later extended to solve the interaction radiation force and torque among multiple spherical objects [11–14].

For other non-spherical objects, the radial distance from the mass center of the object to the locus of any point on the object surface is not a constant. The boundary conditions should be properly described so that the scattered field and the resultant radiation force and torque could be evaluated. Generally, a surface shape function is thus introduced to define the boundary surface of certain geometries, such as spheroid [15] and corrugated circular [16]. Additionally, the radiation effects on the prolate spheroid could be naturally estimated by introducing a spheroidal coordinate system to exactly map the spheroidal surface [17]. The T-matrix method is also commonly applied to investigate the acoustic scattering from non-spherical objects [18], thereby the radiation torque [19]. Alternatively, a promising method to analytically formulate the radiation force and torque is the use of the conformal transformation technique. An asymmetric geometry is mapped to a sphere in the mapping coordinate system [20], where the locus of

* tianquan@connect.hku.hk

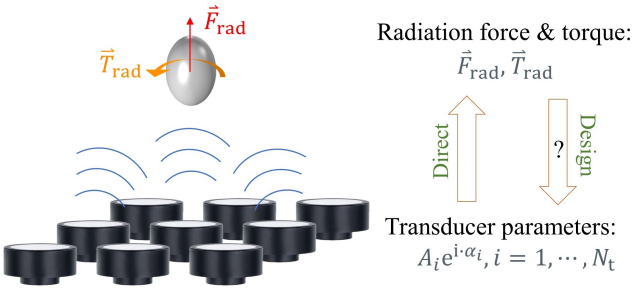

FIG. 1. The direct and design (retrieval) problems. For the direct problems, transducer parameters are given, and the radiation force and torque on a non-spherical particle can be evaluated [22, 29]. For the design (or retrieval) problems, the radiation force and torque are given in advance, while the transducer parameters that result in the desired radiation force and torque are unknown.

all points corresponding to the new radial coordinate being a constant exactly coincides with the scatterer surface. As a result, the boundary conditions can be conveniently enforced, and the radiation force and torque are asymptotically obtainable [21, 22].

Under the dominance of the radiation force and torque, ones can handle objects in a contamination-free and label-free manner [23]. Ultrasound transducer array is widely used in containerless transportation [24, 25] or contactless rotation [26] of micro-objects in the air. Typically, these acoustic tweezers or levitators handle objects with a radius much smaller than the acoustic wavelength. This corresponds to the so-called Rayleigh scattering regime (i.e., the long-wave limit). In this limitation, the scattering contribution is relatively small, and the acoustic radiation potential can be expressed in terms of the external driving fields from transducers. The key to dynamically manipulating these micro-objects is to provide an effective retrieval algorithm [24, 27, 28] that can efficiently retrieve the transducer parameters (amplitude and phase) to obtain the desired spatial potential distribution.

Beyond the Rayleigh regime, the radiation force and torque heavily depend on the shape of the object, since their geometric asymmetry strongly affects the scattering properties [21]. In other words, the geometric features become a potential degree of freedom to tune acoustophoretic processes. The additional radiation force and torque due to geometric asymmetry move the objects and constantly change their positions and orientations. Through embedding the translation and rotation transformations to dynamically evaluate the radiation force and torque on the objects, the time-varying trajectories of the non-spherical objects can be predicted [22], and a graphical user interface (GUI) software is provided to implement prediction once the transducer parameters are given [29].

However, another significant problem is how to retrieve the transducer parameters that exert the desired radiation force and torque on a non-spherical Mie object (Fig. 1). The radiation efficiency here depends not only on the external driving field of the transducer array, but also on the geometric features of the object. Undoubtedly, a systematic approach is demanded to retrieve the transducer parameters, bringing the desired radiation force and torque on the non-spherical objects beyond the Rayleigh range. Recently, a numerical boundary hologram approach was proposed to provide the desired radiation force and torque on a free-shaped object by designing and optimizing the sound field around the object [30]. While they did not analytically and directly related the transducer parameters to the radiation force and torque.

Here, with the aid of the translation addition theorem [31, 32], we rearrange the radiation force and torque into a set of nonlinear partial-wave expressions, which are the quasi-explicit functions of the transducer (phase and amplitude) parameters. By specifying a set of desired radiation force and torque, a corresponding system of nonlinear equations with unknown transducer parameters is presented. Therefore, the problem of obtaining the desired radiation force and torque is simplified to find a feasible solution that fulfills the system of nonlinear equations. Finally, several cases of stable trapping of the non-spherical Mie objects above the transducer array are presented to demonstrate the validity of the partial-wave-based retrieval method.

II. TRANSLATION POTENTIAL FIELD OF A TRANSDUCER ARRAY

With reference to Fig. 1, the time-harmonic acoustic waves generated by an ultrasound transducer array interact with an axisymmetric particle that levitates in an inviscid fluid with c_0 the speed of sound. Each transducer is regarded as a circular radiator, and its wave function can be approximated by the time-harmonic far-field expression of a circular piston vibration source [33]. Here, as illustrated in Fig. 2, the pressure amplitude field generated from

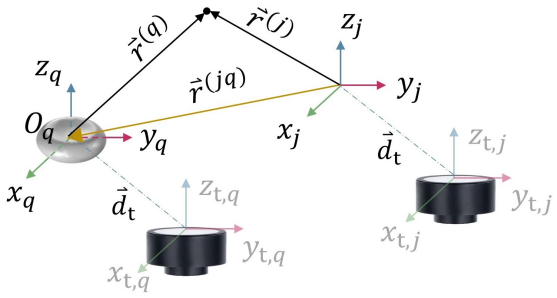

FIG. 2. Geometric description of a particle-transducer system and its positional relationship. A reference coordinate system (O_q) is established in terms of the levitated particle, and the center of mass of the irregular particle is set to coincide with the origin of the reference coordinate system. A transformation is applied to translate the wave function from the transducer systems (coordinates with subscript 't') to their corresponding particle systems with distance vector $\vec{d}_t$. The probe (q-th) system and the source (j-th) system can be related by a position vector $\vec{r}^{(jq)}$, which enables the acoustic potential information of any source system(s) to be expressed on the probe system with the help of the translation addition theorem.

the q-th transducer in terms of its reference coordinate system (O_q) is

$$\hat{p}(\vec{r}^{(q)}) = P_0 \cdot \frac{2\bar{j}_1\left(\frac{kd}{2}\sin\angle\left(\vec{r}^{(q)}+\vec{d}_t\right)\right)}{\frac{kd}{2}\sin\angle\left(\vec{r}^{(q)}+\vec{d}_t\right)} \cdot \frac{\mathrm{e}^{\mathrm{i}k\left|\vec{r}^{(q)}+\vec{d}_t\right|}}{\left|\vec{r}^{(q)}+\vec{d}_t\right|}, \tag{1}$$

where $\vec{r}^{(q)}$ is the observation position vector, and $\vec{d}_t$ is the distance vector between the center of the probe transducer and the mass center of the levitated particle, used to transform the wave function from the transducer system to the particle system. Symbol $\angle(\cdot)$ means the cosine angle of the corresponding vector therein, and power parameter $P_0 = \frac{-\mathrm{i}\rho_0 c_s k d^2 \hat{v}_0}{8}$ (unit: N m^{-1}). Function $\bar{j}_1(\cdot)$ represents the Bessel function of the first kind. It can be found that the transducer is characterized by its diameter d and complex amplitude of the radial velocity $\hat{v}_0$.

For simplicity, the incident and scattered waves are commonly described in terms, respectively, of the velocity potential amplitudes $\hat{\phi}_{\mathrm{ex}}$ (or $\hat{\phi}_{\mathrm{ex}}(\vec{r})$) and $\hat{\phi}_{\mathrm{sc}}$ (or $\hat{\phi}_{\mathrm{sc}}(\vec{r})$), as functions of a position vector $\vec{r}$. These velocity potential amplitude functions satisfy the Helmholtz wave equation $\left(\nabla^2 + k^2\right)\hat{\phi} = 0$, with $\hat{\phi} = \hat{\phi}_{\mathrm{ex}} + \hat{\phi}_{\mathrm{sc}}$. The hat symbol $\hat{}$ represents the complex amplitude of the corresponding variable, and $k = \frac{\omega}{c_0}$ is the wavenumber with ω the angular frequency. For simplicity, the time dependence $\mathrm{e}^{-\mathrm{i}\omega t}$ is omitted. Without loss of generality, we assume that all transducers have the same diameter d, while operating under different ultrasound transducer parameters $A_i\mathrm{e}^{\mathrm{i}\cdot\alpha_i}$ (amplitude A_i and phase α_i of the ultrasound transducer excitation signal), $i = 1, 2, \cdots, N_t$ with the total number of transducers N_t.

With respect to the probe (q-th) transducer, its potential amplitude field $\hat{\phi}^{(q)}_{\mathrm{trans}}$ (or $\hat{\phi}_{\mathrm{trans}}(\vec{r}^{(q)})$) in terms of the q-th coordinates depends on the transducer parameters $A_q\mathrm{e}^{\mathrm{i}\cdot\alpha_q}$ and the observation position vector $\vec{r}^{(q)} = (r^{(q)}, \theta^{(q)}, \varphi^{(q)})$ with the radial distance $r^{(q)}$, polar angle $\theta^{(q)}$, and azimuthal angle $\varphi^{(q)}$. The potential amplitude function could be expanded into a partial-wave series [34], as

$$\hat{\phi}^{(q)}_{\mathrm{trans}} = A_q\mathrm{e}^{\mathrm{i}\cdot\alpha_q}\sum_{n,m} a_{nm} J_n^{m(q)}, \tag{2}$$

where a_{nm} are the beam-shape coefficients, which can be determined by inverting the partial wave series through the orthogonality relation of the spherical harmonics [as given later in Eq. (6)], and $J_n^{m(q)} \equiv j_n(kr^{(q)})Y_n^m(\theta^{(q)}, \varphi^{(q)})$. $j_n(kr^{(q)})$ is the spherical Bessel function of order n at a position $r^{(q)}$ and $Y_n^m(\theta^{(q)}, \varphi^{(q)})$ is the spherical harmonic function of n-th order and m-th degree at the angular position $(\theta^{(q)}, \varphi^{(q)})$. Abbreviation $\sum_{n,m} \equiv \sum_{n=0}^{N}\sum_{m=-n}^{n}$, where N is the truncation number for the summation series. Additionally, as illustrated in Fig. 2, the potential amplitude function from the j-th transducer described in the j-th coordinates can be translated and consistently formulated by the q-th coordinates with the aid of the translation addition theorem [14, 22, 32] and vector relationship of $\vec{r}^{(j)} = \vec{r}^{(q)} + \vec{r}^{(jq)}$,

in which the relative position vector of these two transducers $\vec{r}^{(jq)}$ is given.

$$\begin{aligned}\hat{\phi}_{\text{trans}}^{(j)} &= A_j \mathrm{e}^{\mathrm{i}\cdot\alpha_j} \sum_{n,m} a_{nm} J_n^{m(j)} \\ &= A_j \mathrm{e}^{\mathrm{i}\cdot\alpha_j} \sum_{n,m} a_{nm}^{(j)} J_n^{m(q)},\end{aligned} \tag{3}$$

where $a_{nm}^{(j)} = \sum_{\nu,\mu} a_{\nu\mu} S_{\nu,n}^{\mu,m(1)}(k\vec{r}^{(jq)})$, defined as the translation beam-shape coefficients of the j-th transducer. $S_{\nu,n}^{\mu,m(1)}(k\vec{r}^{(jq)})$ is the separation transform matrix of the first kind [32]. Note that if $j = q$, $a_{nm}^{(q)} = \sum_{\nu,\mu} a_{\nu\mu} S_{\nu,n}^{\mu,m\ (1)}(0) = a_{nm}$.

The total velocity potential amplitude from a whole transducer array can be obtained by a summation of the contributions from all transducers:

$$\hat{\phi}_{\text{ex}} = \sum_{i=1}^{N_{\text{t}}} \hat{\phi}_{\text{trans}}^{(i)} = \sum_{n,m} [a]_{nm} J_n^{m(q)}, \tag{4}$$

where the equivalent beam-shape coefficients $[a]_{nm} = \sum_{i=1}^{N_{\text{t}}} A_i \mathrm{e}^{\mathrm{i}\cdot\alpha_i} a_{nm}^{(i)}$. And the corresponding scattering potential amplitude in the far-field can be expressed in terms of a partial wave series as:

$$\hat{\phi}_{\text{sc}} = \sum_{n,m} s_{nm} [a]_{nm} H_n^{m(q)}, \tag{5}$$

where s_{nm}, the scalar scattering coefficients, are determined by the acoustic properties of the object and the surrounding fluid, as well as the geometric features of the levitated object [refer to Eqs. (7) and (8)].

III. EXPANSION COEFFICIENTS

The acoustic pressure amplitude function generated from a circular radiator in the corresponding particle coordinate system follows Eq. (1), and it can be connected to its velocity potential amplitude field by $\hat{\phi}_{\text{trans}}(\vec{r}) = \mathrm{i}\frac{\hat{p}(\vec{r})}{\omega\rho_0}$. The beam-shape coefficients defined in Eq. (2) may be numerically evaluated through the orthogonality properties of the spherical harmonics:

$$a_{nm} = \frac{1}{j_n(k\mathrm{R})} \int_0^{2\pi} \int_0^{\pi} \hat{\phi}_{\text{trans}}(\vec{\mathrm{R}}) Y_n^m(\theta,\varphi)^* \sin\theta \mathrm{d}\theta \mathrm{d}\varphi, \tag{6}$$

where $\vec{\mathrm{R}} = (\mathrm{R}, \theta, \varphi)$ specifies a spherical space with a radius of R that contains the scatterer, not the sound sources. The superscript symbol $\cdot^*$ means taking conjugation of the corresponding variable.

On the other hand, the scaled scattering coefficients defined in Eq. (5) will be determined by applying appropriate boundary conditions to the fluid-particle interface [21, 22]. For Dirichlet (sound-soft) and Neumann (sound-hard) boundary conditions, the scaled scattering coefficients are solved, respectively, by the following matrices

$$\begin{aligned}&\sum_{n=0}^{\infty} [a]_{nm'} \Gamma_n^{n',m'} + \sum_{n=0}^{\infty} s_{nm'} [a]_{nm'} \Lambda_n^{n',m'} = 0, \\ &(n' = 0, 1, \cdots, \infty; m' = -\infty, \cdots, 0, \cdots, \infty)\end{aligned} \tag{7}$$

and

$$\begin{aligned}&\sum_{n=0}^{\infty} [a]_{nm'} \Gamma_{n,u}^{n',m'} + \sum_{n=0}^{\infty} s_{nm'} [a]_{nm'} \Lambda_{n,u}^{n',m'} = 0. \\ &(n' = 0, 1, \cdots, \infty; m' = -\infty, \cdots, 0, \cdots, \infty)\end{aligned} \tag{8}$$

Here, the structural functions, $\Gamma_n^{n',m'}$ and $\Lambda_n^{n',m'}$, and their partial derivatives along the radial coordinate, u, under the mapping system, $\Gamma_{n,u}^{n',m'}$ and $\Lambda_{n,u}^{n',m'}$, are given in Eqs. (A4) and (A5) of Appendix A. A detailed derivation of the above matrices is given in Appendix B of our previous work [22], where the conformal transformation approach is applied to map the axisymmetric geometries in physical space to a sphere in mapped space, denoted as a quasi-spherical

coordinate system with u, w, and v, respectively, for the radial, polar angular, and azimuthal angular coordinates. In this way, the separation of variables can be employed to solve the corresponding Helmholtz wave equation subjecting to the spherical boundary conditions in the mapping coordinate system [21]. Note that these structural functions contain the geometric features of the non-spherical objects during the mapping process, and thus the scalar scattering coefficients inherit these geometric asymmetric features through the matrix (7) or (8). Note that merely sound-hard or sound-soft materials are considered in this study. It can be conveniently extended to calculate the scalar scattering coefficients for the compressible objects (with Cauchy boundary condition) satisfying that the pressure and particle velocity of the exterior and interior surfaces of the scatterer are equal.

IV. ACOUSTIC RADIATION FORCE AND TORQUE

The acoustic radiation force and torque are caused by the transfer of, respectively, the time-averaged momentum flux and angular momentum flux to the object [2, 3]. By integrating these time-averaged fluxes projected onto the normal vector over the surface of the geometry, the radiation force and torque exerted on an axisymmetric irregular object can be asymptotically obtained under the Cartesian coordinates [21, 22], as

$$\begin{aligned} F_x &= -\frac{\rho_0}{4}\mathrm{Im}\left\{\mathbf{A}-\mathbf{B}+\mathbf{C}-\mathbf{D}\right\},\\ F_y &= +\frac{\rho_0}{4}\mathrm{Re}\left\{\mathbf{A}-\mathbf{B}-\mathbf{C}+\mathbf{D}\right\},\\ F_z &= -\frac{\rho_0}{2}\mathrm{Im}\left\{\mathbf{E}-\mathbf{F}\right\}, \end{aligned} \tag{9}$$

$$\begin{aligned} T_x &= +\frac{\rho_0}{4k}\mathrm{Re}\left\{\mathbf{G}+\mathbf{H}\right\},\\ T_y &= +\frac{\rho_0}{4k}\mathrm{Im}\left\{\mathbf{G}-\mathbf{H}\right\},\\ T_z &= +\frac{\rho_0}{2k}\mathrm{Re}\left\{\mathbf{I}\right\}, \end{aligned} \tag{10}$$

and

$$\begin{aligned} \mathbf{A} &= \sum_{n,m} A_{n+1}^{m+1}\left([a]_{nm}+[a]_{nm}s_{nm}\right)\left([a]_{n+1,m+1}s_{n+1,m+1}\right)^*,\\ \mathbf{B} &= \sum_{n,m} B_{n-1}^{m+1}\left([a]_{nm}+[a]_{nm}s_{nm}\right)\left([a]_{n-1,m+1}s_{n-1,m+1}\right)^*,\\ \mathbf{C} &= \sum_{n,m} C_{n+1}^{m-1}\left([a]_{nm}+[a]_{nm}s_{nm}\right)\left([a]_{n+1,m-1}s_{n+1,m-1}\right)^*,\\ \mathbf{D} &= \sum_{n,m} D_{n-1}^{m-1}\left([a]_{nm}+[a]_{nm}s_{nm}\right)\left([a]_{n-1,m-1}s_{n-1,m-1}\right)^*,\\ \mathbf{E} &= \sum_{n,m} E_{n+1}^{m}\left([a]_{nm}+[a]_{nm}s_{nm}\right)\left([a]_{n+1,m}s_{n+1,m}\right)^*,\\ \mathbf{F} &= \sum_{n,m} F_{n-1}^{m}\left([a]_{nm}+[a]_{nm}s_{nm}\right)\left([a]_{n-1,m}s_{n-1,m}\right)^*,\\ \mathbf{G} &= \sum_{n,m} G_{n}^{m}\left([a]_{nm}+[a]_{nm}s_{nm}\right)\left([a]_{n,m+1}s_{n,m+1}\right)^*,\\ \mathbf{H} &= \sum_{n,m} G_{n}^{-m}\left([a]_{nm}+[a]_{nm}s_{nm}\right)\left([a]_{n,m-1}s_{n,m-1}\right)^*,\\ \mathbf{I} &= \sum_{n,m} m\left([a]_{nm}+[a]_{nm}s_{nm}\right)\left([a]_{nm}s_{nm}\right)^*. \end{aligned} \tag{11}$$

where operators $\mathrm{Re}\{\cdot\}$ and $\mathrm{Im}\{\cdot\}$ mean taking the real and imaginary parts of the expression, respectively. The weighting coefficients A_n^m, B_n^m, C_n^m, D_n^m, E_n^m, F_n^m, and G_n^m are given in Eq. (B2) of Appendix B.

In Eqs. (9) and (10), the existence of real and imaginary operators brings additional complexity to describe the relationship between the transducer parameters and the radiation force and torque. To eliminate the real and

imaginary operators, we first decompose the expansion coefficients as their complex expressions by $a_{nm}^{(i)} = \alpha_{nm}^{(i)} + \mathrm{i}\cdot\beta_{nm}^{(i)}$ and $s_{nm} = \sigma_{nm} + \mathrm{i}\cdot\epsilon_{nm}$. Then, the combination coefficients can be described as

$$\begin{aligned}
&\left(a_{nm}^{(i)} + a_{nm}^{(i)} s_{nm}\right)\left(a_{vu}^{(j)} s_{vu}\right)^{*} = R_{n,v}^{m,u(ij)} + \mathrm{i}\cdot I_{n,v}^{m,u(ij)}, \\
&\begin{cases} R_{n,v}^{m,u(ij)} = \left(\alpha_{nm}^{(i)} + \tau_{nm}^{(i)}\right)\tau_{vu}^{(j)} + \left(\beta_{nm}^{(i)} + \eta_{nm}^{(i)}\right)\eta_{vu}^{(j)} \\ I_{n,v}^{m,u(ij)} = \left(\beta_{nm}^{(i)} + \eta_{nm}^{(i)}\right)\tau_{vu}^{(j)} - \left(\alpha_{nm}^{(i)} + \tau_{nm}^{(i)}\right)\eta_{vu}^{(j)} \end{cases},
\end{aligned} \tag{12}$$

where $\tau_{nm}^{(i)} = \alpha_{nm}^{(i)}\sigma_{nm} - \beta_{nm}^{(i)}\epsilon_{nm}$ and $\eta_{nm}^{(i)} = \beta_{nm}^{(i)}\sigma_{nm} + \alpha_{nm}^{(i)}\epsilon_{nm}$. Then, with the help of Eq. (12), further considering the definition of the equivalent beam-shape coefficients $[a]_{nm} = \sum_{i=1}^{N_\mathrm{t}} A_i \mathrm{e}^{\mathrm{i}\cdot\alpha_i} a_{nm}^{(i)}$ and the relationship of $A_i\mathrm{e}^{\mathrm{i}\cdot\alpha_i}\cdot(A_j\mathrm{e}^{\mathrm{i}\cdot\alpha_j})^{*} = A_iA_j[\cos(\alpha_i-\alpha_j) + \mathrm{i}\cdot\sin(\alpha_i-\alpha_j)]$, equation (11) could be rearranged as follows:

$$\begin{aligned}
\mathbf{A} &= \sum_{n,m}\sum_{i=1}^{N_\mathrm{t}}\sum_{j=1}^{N_\mathrm{t}} A_iA_jA_{n+1}^{m+1}Z_{n,n+1}^{m,m+1(ij)}, \\
\mathbf{B} &= \sum_{n,m}\sum_{i=1}^{N_\mathrm{t}}\sum_{j=1}^{N_\mathrm{t}} A_iA_jB_{n-1}^{m+1}Z_{n,n-1}^{m,m+1(ij)}, \\
\mathbf{C} &= \sum_{n,m}\sum_{i=1}^{N_\mathrm{t}}\sum_{j=1}^{N_\mathrm{t}} A_iA_jC_{n+1}^{m-1}Z_{n,n+1}^{m,m-1(ij)}, \\
\mathbf{D} &= \sum_{n,m}\sum_{i=1}^{N_\mathrm{t}}\sum_{j=1}^{N_\mathrm{t}} A_iA_jD_{n-1}^{m-1}Z_{n,n-1}^{m,m-1(ij)}, \\
\mathbf{E} &= \sum_{n,m}\sum_{i=1}^{N_\mathrm{t}}\sum_{j=1}^{N_\mathrm{t}} A_iA_jE_{n+1}^{m}Z_{n,n+1}^{m,m(ij)}, \\
\mathbf{F} &= \sum_{n,m}\sum_{i=1}^{N_\mathrm{t}}\sum_{j=1}^{N_\mathrm{t}} A_iA_jF_{n-1}^{m}Z_{n,n-1}^{m,m(ij)}, \\
\mathbf{G} &= \sum_{n,m}\sum_{i=1}^{N_\mathrm{t}}\sum_{j=1}^{N_\mathrm{t}} A_iA_jG_{n}^{m}Z_{n,n}^{m,m+1(ij)}, \\
\mathbf{H} &= \sum_{n,m}\sum_{i=1}^{N_\mathrm{t}}\sum_{j=1}^{N_\mathrm{t}} A_iA_jG_{n}^{-m}Z_{n,n}^{m,m-1(ij)}, \\
\mathbf{I} &= \sum_{n,m}\sum_{i=1}^{N_\mathrm{t}}\sum_{j=1}^{N_\mathrm{t}} A_iA_jmZ_{n,n}^{m,m(ij)},
\end{aligned} \tag{13}$$

where

$$\begin{aligned}
Z_{n,v}^{m,u(ij)} = &\left[\cos\left(\alpha_i-\alpha_j\right)R_{n,v}^{m,u(ij)} - \sin\left(\alpha_i-\alpha_j\right)I_{n,v}^{m,u(ij)}\right] \\
&+\mathrm{i}\ \cdot\ \left[\sin\left(\alpha_i-\alpha_j\right)R_{n,v}^{m,u(ij)} + \cos\left(\alpha_i-\alpha_j\right)I_{n,v}^{m,u(ij)}\right].
\end{aligned} \tag{14}$$

Through inserting Eq. (13) into Eqs. (9) and (10), we obtain expressions for the radiation force and torque, which

directly depend on the transducer parameters without involving real and imaginary operators, as:

$$\begin{aligned}
F_x &= -\frac{\rho_0}{4}\sum_{i,j=1}^{N_\mathrm{t}} A_i A_j \left[\sin\left(\alpha_{ij}\right) M_{Fx}^{(ij)} + \cos\left(\alpha_{ij}\right) N_{Fx}^{(ij)}\right], \\
F_y &= +\frac{\rho_0}{4}\sum_{i,j=1}^{N_\mathrm{t}} A_i A_j \left[\cos\left(\alpha_{ij}\right) M_{Fy}^{(ij)} - \sin\left(\alpha_{ij}\right) N_{Fy}^{(ij)}\right], \\
F_z &= -\frac{\rho_0}{2}\sum_{i,j=1}^{N_\mathrm{t}} A_i A_j \left[\sin\left(\alpha_{ij}\right) M_{Fz}^{(ij)} + \cos\left(\alpha_{ij}\right) N_{Fz}^{(ij)}\right],
\end{aligned} \tag{15}$$

$$\begin{aligned}
T_x &= +\frac{\rho_0}{4k}\sum_{i,j=1}^{N_\mathrm{t}} A_i A_j \left[\cos\left(\alpha_{ij}\right) M_{Tx}^{(ij)} - \sin\left(\alpha_{ij}\right) N_{Tx}^{(ij)}\right], \\
T_y &= +\frac{\rho_0}{4k}\sum_{i,j=1}^{N_\mathrm{t}} A_i A_j \left[\sin\left(\alpha_{ij}\right) M_{Ty}^{(ij)} + \cos\left(\alpha_{ij}\right) N_{Ty}^{(ij)}\right], \\
T_z &= +\frac{\rho_0}{2k}\sum_{i,j=1}^{N_\mathrm{t}} A_i A_j \left[\cos\left(\alpha_{ij}\right) M_{Tz}^{(ij)} - \sin\left(\alpha_{ij}\right) N_{Tz}^{(ij)}\right],
\end{aligned} \tag{16}$$

where abbreviations $\sum_{i,j=1}^{N_\mathrm{t}} \equiv \sum_{i=1}^{N_\mathrm{t}}\sum_{j=1}^{N_\mathrm{t}}$ and $\alpha_{ij} = (\alpha_i - \alpha_j)$, and the characteristic coefficients $M_{Fx}^{(ij)}$, $N_{Fx}^{(ij)}$, $M_{Fy}^{(ij)}$, $N_{Fy}^{(ij)}$, $M_{Fz}^{(ij)}$, $N_{Fz}^{(ij)}$, $M_{Tx}^{(ij)}$, $N_{Tx}^{(ij)}$, $M_{Ty}^{(ij)}$, $N_{Ty}^{(ij)}$, $M_{Tz}^{(ij)}$, and $N_{Tz}^{(ij)}$ are listed in Eq. (B1) of Appendix B.

V. LYAPUNOV STABILITY CONDITIONS

To discuss the trapping stability, the Lyapunov stability theorem [35] is applied. We here consider a single object that is trapped at a potential equilibrium position. Considering that the axisymmetric objects tend to tune their orientations (by the additional radiation torque due to geometric asymmetry) and remain stable when their symmetry of axis is parallel or perpendicular to the direction of wave propagation [21], only the positional stability is analyzed. When all the forces exerted on the object balance and the viscous damping from the medium can be ignored, the equation of motion becomes

$$m\frac{\mathrm{d}^2\Delta\vec{r}}{\mathrm{d}t^2} - \nabla\vec{F}\cdot\Delta\vec{r} = 0, \tag{17}$$

where m represents the mass of the objects, and $\Delta\vec{r}$ is the disturbance of the object from its equilibrium position. In the Lyapunov sense, the stability is fully governed by the eigenvalues $\nabla\vec{F}$, which should be non-positive real numbers [30] for stable trapping. In this way, the minor fluctuations will gradually dissipate, thus maintaining the trapping stability. Here, the stability along the x-, the y-, and the z-axes are discussed:

$$\frac{\partial F_i}{\partial i} < 0; i = x, y, z, \tag{18}$$

where F_i means the radiation force along the i-axis, referred to Eq. (15).

VI. SYSTEM OF NONLINEAR EQUATIONS FOR RETRIEVED TRANSDUCER PARAMETERS

One can specify the desired radiation force, $\vec{F}_\mathrm{s} = (F_{\mathrm{s},x}, F_{\mathrm{s},y}, F_{\mathrm{s},z})$, and radiation torque, $\vec{T}_\mathrm{s} = (T_{\mathrm{s},x}, T_{\mathrm{s},y}, T_{\mathrm{s},z})$ in Eqs. (15) and (16), and then the transducer parameters may be retrieved by solving the system of nonlinear equations.

Generally, the governing system becomes

$$
\begin{aligned}
F_{\mathrm{s},x} &= -\frac{\rho_0}{4}\sum_{i,j=1}^{N_\mathrm{t}} A_i A_j \left[\sin\left(\alpha_{ij}\right) M_{Fx}^{(ij)} + \cos\left(\alpha_{ij}\right) N_{Fx}^{(ij)}\right], \\
F_{\mathrm{s},y} &= +\frac{\rho_0}{4}\sum_{i,j=1}^{N_\mathrm{t}} A_i A_j \left[\cos\left(\alpha_{ij}\right) M_{Fy}^{(ij)} - \sin\left(\alpha_{ij}\right) N_{Fy}^{(ij)}\right], \\
F_{\mathrm{s},z} &= -\frac{\rho_0}{2}\sum_{i,j=1}^{N_\mathrm{t}} A_i A_j \left[\sin\left(\alpha_{ij}\right) M_{Fz}^{(ij)} + \cos\left(\alpha_{ij}\right) N_{Fz}^{(ij)}\right], \\
T_{\mathrm{s},x} &= +\frac{\rho_0}{4k}\sum_{i,j=1}^{N_\mathrm{t}} A_i A_j \left[\cos\left(\alpha_{ij}\right) M_{Tx}^{(ij)} - \sin\left(\alpha_{ij}\right) N_{Tx}^{(ij)}\right], \\
T_{\mathrm{s},y} &= +\frac{\rho_0}{4k}\sum_{i,j=1}^{N_\mathrm{t}} A_i A_j \left[\sin\left(\alpha_{ij}\right) M_{Ty}^{(ij)} + \cos\left(\alpha_{ij}\right) N_{Ty}^{(ij)}\right], \\
T_{\mathrm{s},z} &= +\frac{\rho_0}{2k}\sum_{i,j=1}^{N_\mathrm{t}} A_i A_j \left[\cos\left(\alpha_{ij}\right) M_{Tz}^{(ij)} - \sin\left(\alpha_{ij}\right) N_{Tz}^{(ij)}\right], \\
&\frac{\partial F_i}{\partial i} < 0; i = x, y, z,
\end{aligned}
\tag{19}
$$

Note that there are six independent equations and three stability conditions presented in Eq. (19), while the number of the unknown variables is up to $2 \times N_\mathrm{t}$ (N_t amplitude parameter and N_t phase parameters). To solve the non-square system (of the first six equations), a well-established Levenberg-Marquardt algorithm [36, 37] is applied. There are numerous feasible solutions, and these solutions are significantly sensitive to the initial values of the transducer parameters. The last three inequalities are used to find stable solutions from all the feasible results. Furthermore, the above system can also be designed as an optimization problem: find the amplitude and phase distributions by minimizing the stability conditions while maintaining the force and torque balance. This optimization problem is solvable using the BFGS algorithm [26, 30].

It should be emphasized that the characteristic coefficients in Eq. (B1) are directly dependent on the beam-shape coefficients, a_{nm}, and the scalar scattering coefficients, s_{nm} [since $R_{n,v}^{m,u(ij)}$ and $I_{n,v}^{m,u(ij)}$ depend on $a_{nm}^{(i)}$, $a_{vu}^{(j)}$, and s_{nm} through Eq. (12), and $a_{nm}^{(i)}$ or $a_{vu}^{(j)}$ is a function of a_{nm} through Eq. (3)]. From Eq. (6), it can be found that a_{nm} are independent of the transducer parameters. It can be further proven that for the spherical objects, scalar scattering coefficients s_{nm} are reduced to s_n, and are not dependent on the properties of the incident wave, as given in Eq. (7) of [38] and Eq. (21) of [14] for rigid and compressible objects, and Eq. (30) of [39] for viscoelastic objects. Hence, for the sphere, s_{nm} are not dependent on the transducer parameters, equation (19) is an explicit system in terms of the transducer parameters. In this way, the transducer parameters to create the desired radiation force and torque on an object could be directly obtained by solving Eq. (19) in terms of the unknown transducer parameters. Unfortunately, for a general axisymmetric geometry, s_{nm} are nonlinearly related to $[a]_{nm}$ by matrix (7) or (8), while $[a]_{nm}$ involve the contributions from the whole transducer array. As a result, s_{nm} are functions of the transducer parameters, and Eq. (19) is never an explicit system in terms of the transducer parameters.

Considering that s_{nm} are related to the transducer parameters for the non-spherical objects, we employ an iterative algorithm to dynamically update s_{nm}. The flowchart is summarized in Fig. 3. To engineer the desired radiation force and torque (denoted as $\vec{F}_\mathrm{s}$ and $\vec{T}_\mathrm{s}$) on a levitated object, we need to initialize the inputting transducer parameters (amplitude $\bar{A}_i$ and phase $\bar{\alpha}_i$), used to determine the equivalent beam-shape coefficients, $[a]_{nm}$, and the scalar scattering coefficients, s_{nm}, for the current iterative step. Then, the characteristic coefficients can be obtained to establish the system of nonlinear equations (Eq. (19)), which is used to solve the retrieved transducer parameters (amplitude $\tilde{A}_i$ and phase $\tilde{\alpha}_i$). The retrieved radiation force and torque ($\vec{F}$ and $\vec{T}$) are next evaluated by Eqs. (9) and (10) using $\tilde{A}_i$ and $\tilde{\alpha}_i$. Finally, quantify the deviations between the desired and the retrieved data to determine if the iterative process is complete:

$$
\begin{aligned}
&\begin{cases} \mathrm{err}(\bar{A}_i, \tilde{A}_i) = \left|\frac{\bar{A}_i - \tilde{A}_i}{\xi}\right| \\ \mathrm{err}(\bar{\alpha}_i, \tilde{\alpha}_i) = \left|\frac{\bar{\alpha}_i - \tilde{\alpha}_i}{2\pi}\right| \end{cases}, \\
&\mathrm{err} = \max\left[\mathrm{err}(\bar{A}_i, \tilde{A}_i), \mathrm{err}(\bar{\alpha}_i, \tilde{\alpha}_i)\right],
\end{aligned}
\tag{20}
$$

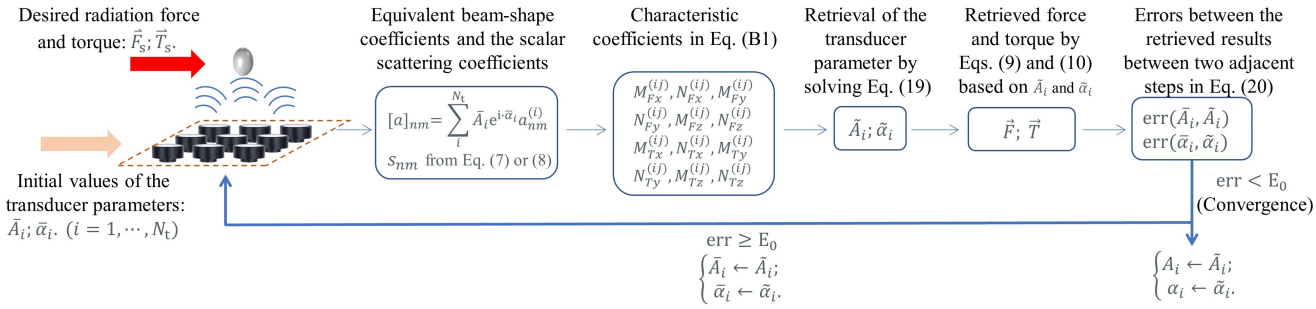

FIG. 3. Flowchart of iteration for transducer parameters to desirably engineer the acoustic radiation force and torque on a non-spherical object. Iteratively adjustment of the transducer parameters: at each iterative step, a series of expansion coefficients are firstly calculated based on the transducer parameters retrieved in the previous step (or initial transducer parameters), and these coefficients are used to solve the transducer parameters of the current step. The newly retrieved transducer parameters are then employed to evaluate the radiation force and torque directly. Finally, the iterative errors are calculated to determine if the iteration is convergent.

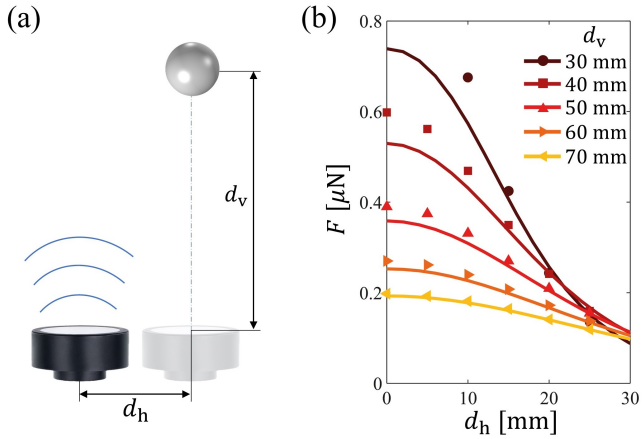

FIG. 4. (a) Schematic diagram of the sphere-transducer system. (b) Theoretical (solid lines) and numerical calculations (symbols) of the radiation force exerted on the sound-hard sphere, as a function of distance vector $\vec{d_t} = (d_h, 0, d_v)$. The radial velocity of transducers is set to $\hat{v}_0 = 1.5$ m/s, and the amplitude and phase parameters are 1 and 0 rad, respectively.

where ξ is a relaxation factor. Here, when err is less than a threshold, said $E_0 = 0.5\%$ for $\xi = 1$, the iterative process is convergent; otherwise, we replace the inputting transducer parameters with the newly retrieved transducer parameters for the next iteration.

VII. ACOUSTIC TRAPS: ENGINEERING THE RADIATION FORCE AND TORQUE

A. Model preparation and validation

We would like to minimize the transducers used in later analysis to save computational resources. Therefore, the sensitivity of the radiation force and geometric position of a transducer is discussed.

A sphere with a radius of $a = 2$ mm is placed above a transducer with a diameter of $d = 10$ mm. The distance vector $\vec{d_t} = (d_h, 0, d_v)$, where vertical and horizontal distances are d_v and d_h, respectively, as illustrated in Fig. 4(a). Here, the transducer works at amplitude parameter $A = 1$ and phase parameter $\alpha = 0$ rad. With the increase of distances d_v and/or d_h, the total radiation force F exerted on the sphere decreases, as shown in Fig. 4(b). The radiation force is evaluated using Eq. (9) [solid lines in Fig. 4(b)] with the truncation number of $N = 12$ [21], and the codes are open-accessed in Soundiation [29]. By contrast, the radiation force and torque based on the finite element method (FEM) [symbols in Fig. 4(b)] are provided to validate the accuracy of Soundiation. It can be observed from Fig. 4(b)

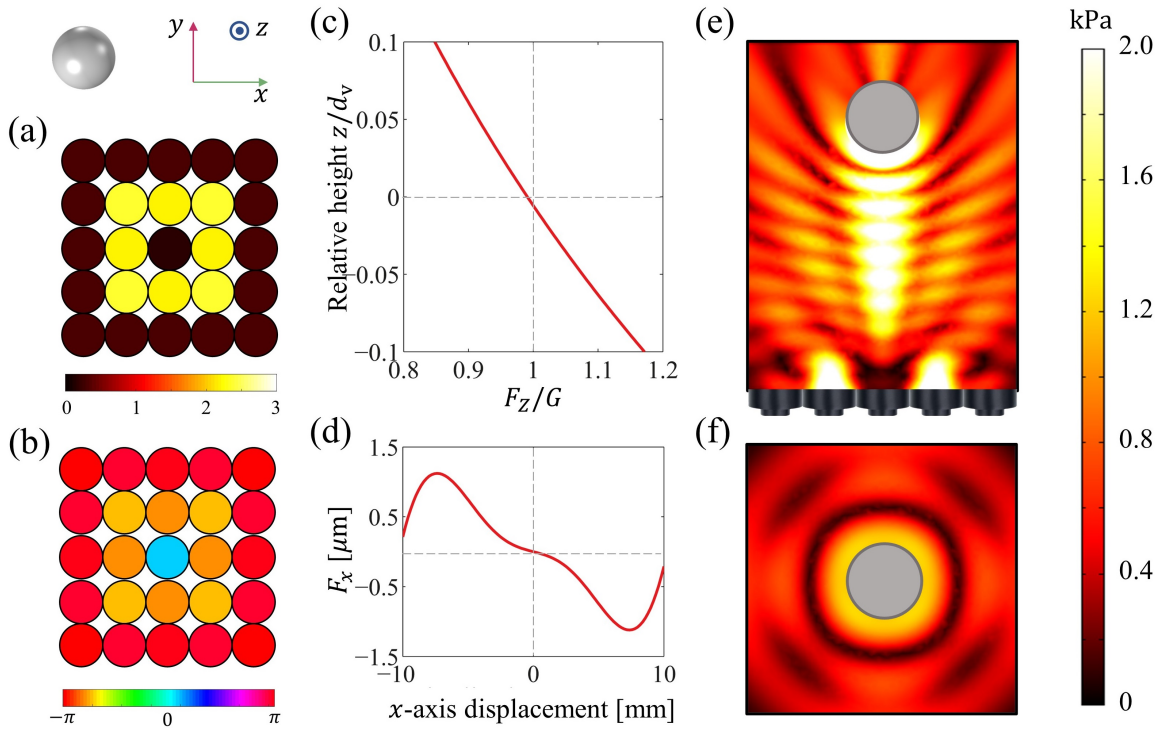

FIG. 5. Stable trapping of a sphere with a radius of $a = 7$ mm above the center of a 5×5 array with a vertical distance of $d_v = 50$ mm. The distributions of the retrieved (a) amplitude parameters and (b) phase parameters for levitations of a sphere by a single-sided 5×5 array; the detailed values are listed in Tab. I. (c) x-axis displacement versus x-axis radiation force applied to a sphere. (d) Relative displacement in z-axis versus the axial radiation force F_z applied to a sphere (dimensionless with gravity G). Absolute acoustic pressure of field simulated by FEM on (e) xz-plane and (f) xy-plane when the array works at the transducer parameters given in (a) and (b).

that the radiation force between our Soundiation and the FEM results are basically matched in the far-field region. While there are some perceivable discrepancies when the distance between the object and the transducer gets smaller (near-field region), this is because Eq. (1) holds when the object is far away from the circular radiator (far-field region). We can find that the radiation force becomes tiny and insensitive when d_h is greater than 25 mm, so we apply a 5×5 transducer array with the object levitated above its center as an example for the later demonstrations.

It should be emphasized that the computational performance of Soundiation has been fully discussed in [21, 22], which presents superior computational accuracy, high geometric adaptivity, and good robustness to various geometric features, while much less computational cost compared with the FEM using commercial software, such as COMSOL Multiphysics. Hence, in the discussion and analysis that follows, Soundiation is used to evaluate the radiation force and torque ($\vec{F}$ and $\vec{T}$) to save the computational time.

B. Retrieved transducer parameters and trapping stability

This section retrieves the transducer parameters by solving Eq. (19) following the iterative process [Fig. 3] to stably trap the non-spherical Mie objects above a 5×5 transducer array. The levitated objects are placed right above the center of the array with a distance vector of $\vec{d}_t = (0, 0, 50)$ mm (i.e., vertical distance of $d_v = 50$ mm). The symmetric axis of the object is set to coincide with the z-axis. All transducers are compactly arranged as a square array, and these circular radiators have the same diameter of $d = 10$ mm and all work at a frequency of 40 kHz. The gravity of these objects can be approximately expressed as $G \approx \frac{4}{3}\pi a^3 \rho_p g$, with $a = 7$ mm its averaged radius and $\rho_p = 30$ kg/m^3 its density (expanded polystyrene particles [24, 26]). The necessary conditions for rigid-body trapped are as follows: (1) the external forces, which are typically gravity and the acoustic radiation force, must be balanced; and (2) the net moment must be zero. Therefore, the non-rotational trapping of the levitated object is equivalent to the cases where

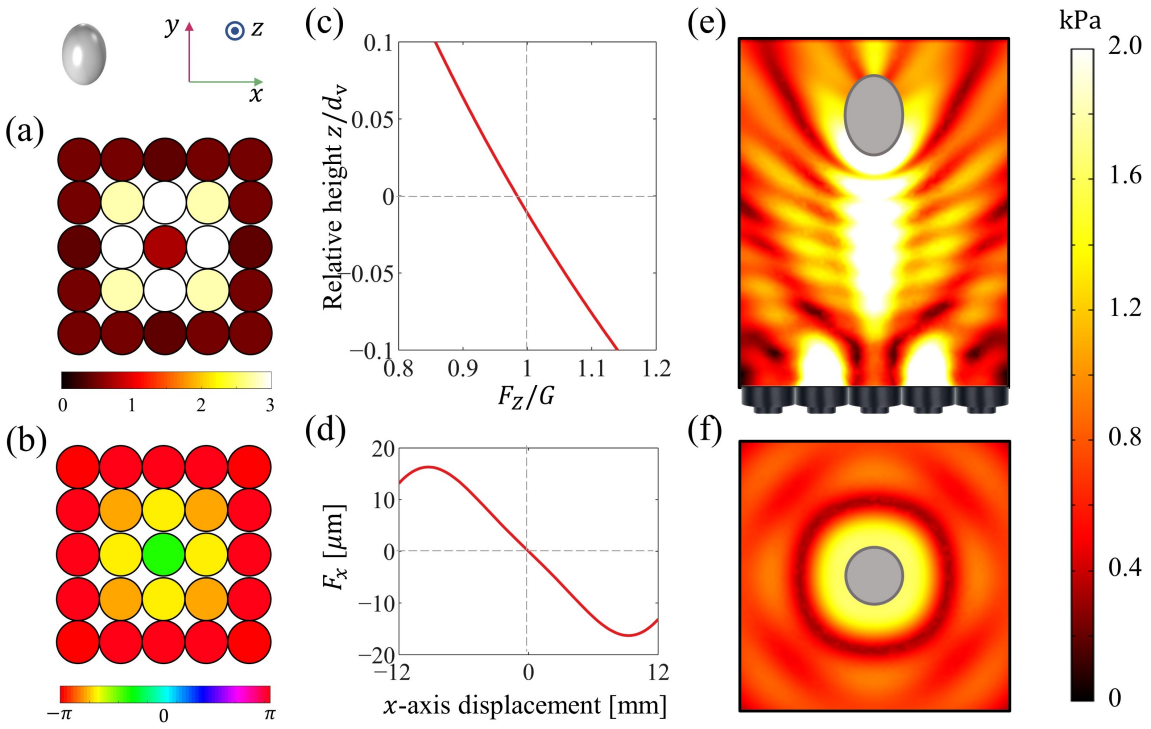

FIG. 6. Stable trapping of a spheroid with an averaged radius of $a = 7$ mm above the center of a 5×5 array with a vertical distance of $d_v = 50$ mm. The geometric feature is specified by the mapping coefficients $c_n = [a, 0, a/5]$, referred to Appendix A and [21, 22]. (a)-(f) The same as described in Fig. 5, but the levitated object is a spheroid.

the desired radiation force and torque are, respectively, $\vec{F}_s = (0, 0, G)$ and $\vec{T}_s = (0, 0, 0)$. Additionally, the Lyapunov stability conditions should be satisfied for a stable equilibrium state, which are constrained in the governing equations [in Eq. (19)].

The retrieved amplitude and phase patterns are illustrated in sub-figures (a) and (b) of Figs. 5, 6, and 7 for the sphere, the spheroid, and the disk, respectively. Correspondingly, the detailed retrieved data is listed in Tab. I. Both the amplitude and phase patterns are symmetric and similar to that of a bottle trap [26]. Considering the symmetries of the patterns and the objects, the radiation torques vanish. Here, the objects are designed to be trapped above the array at a height of $d_v = 50$ mm. As can be found in sub-figure (c) of Figs. 5, 6, and 7, when the axial distance z increases, the axial radiation force (F_z) exerted on the objects becomes smaller than their gravity (G) and vice versa. As a result, the axial restoring force remains sufficient to balance the pushing force and achieves dynamic stability at the targeting height (or axial equilibrium position) around $z/d_v = 0$. Similarly, to realize horizontal stability, a restoring force should be generated against positional fluctuation. As shown in sub-figure (d) of Figs. 5, 6, and 7, the radiation force (i.e., the restoring force) exerted on the objects against the displacement around the horizontal equilibrium positions [satisfying the stability condition in Eq. (18)], which eventually balance and stabilize at the targeting points. Considering the axisymmetric physics in x- and y-directions, we only analyze the motion balance in x-direction. Sub-figures (e) and (f) of Figs. 5, 6, and 7 show a FEM simulation of the absolute acoustic pressure of the sphere, the spheroid, and the disk levitation fields on the vertical xz-plane and horizontal xy-plane. It is apparent that the target objects are surrounded by a higher amplitude pressure field, which remains the object levitated in a stable equilibrium position. Note that these FEM simulations are implemented on COMSOL Multiphysics 5.5.

To check the validity of the retrieved transducer parameters (in Figs. 5, 6, and 7), one can evaluate the radiation force and torque ($\vec{F}$ and $\vec{T}$) using Eqs. (9) and (10) based on the retrieved transducer parameters, and compare these results with the desired force and torque ($\vec{F}_s$ and $\vec{T}_s$). A dimensionless error $\mathrm{err}_{\mathrm{FT}}$ is introduced to quantify the

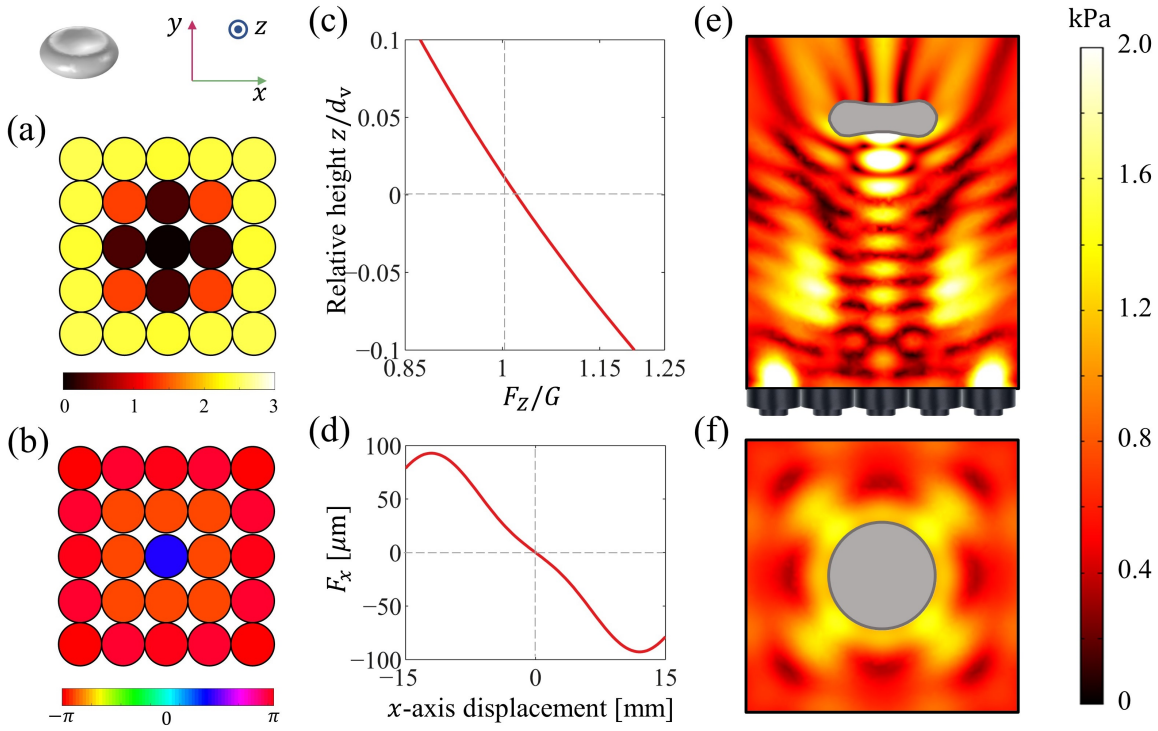

FIG. 7. Stable trapping of a disk with an averaged radius of $a = 7$ mm above the center of a 5×5 array with a vertical distance of $d_v = 50$ mm. The geometric feature is specified by the mapping coefficients $c_n = [a, 0, -a/2, 0, -a/10, 0, -a/30]$, referred to Appendix A and [21, 22]. (a)-(f) The same as described in Fig. 5, but the levitated object is a disk.

retrieved performance:

$$\begin{aligned} &\begin{cases} \mathrm{err}(\vec{F}_\mathrm{s}, \vec{F}) = \left| \frac{\vec{F} - \vec{F}_\mathrm{s}}{G} \right| \\ \mathrm{err}(\vec{T}_\mathrm{s}, \vec{T}) = \left| \frac{\vec{T} - \vec{T}_\mathrm{s}}{G/k} \right| \end{cases}, \\ &\mathrm{err}_\mathrm{FT} = \max\left[\mathrm{err}(\vec{F}_\mathrm{s}, \vec{F}), \mathrm{err}(\vec{T}_\mathrm{s}, \vec{T}) \right], \end{aligned} \tag{21}$$

and estimated errors are listed in Tab. I. It can be seen that the errors are smaller than 5%. Generally, the number of iterations required to reach a solution is dependent to the initial values of the amplitude and phase parameters ($\bar{A}_i$ and $\bar{\alpha}_i$), and these processes typically converge within 10 iteration steps, and each step will take around 1 to 5 mins, depending on the number of the transducers.

Experimentally, the acoustic delay-lines method [40] can be used to realize different distribution of the phase parameters (α_i). The different distribution of the amplitude parameters (A_i) can be achieved by applying different voltages to the transducers. The acoustic pressure amplitude field of each transducer depends on the radial velocity $\hat{v}_0$ [based on Eq. (1)], and the final pressure amplitude field is a linear product with the amplitude parameters (A_i) [referred to Eqs. (2) and (3)]. Hence, the operating radial velocity should be proportional to the amplitude parameters as $\hat{v}_i = \hat{v}_0 A_i$. Considering that the radial velocity is a function of the applied voltages to the transducers, $\hat{v} = f(U)$, it is possible to tune the applied voltages (U) on the array to modulate the distribution of amplitude parameters. Note that the solutions listed in Figs. 5, 6, and 7 are merely one of the numerous feasible solutions. The existence of a solution is not always guaranteed. That is, a solution satisfying the constraints cannot be found when the conditions are physically unfeasible, or the objects are too complex for the given array. For example, for the non-axisymmetric Mie objects, the retrieved transducer patterns are generally non-symmetric to balance the additional radiation torque due to the geometric asymmetry. While the asymmetry of the incident wavefield will inevitably bring an unbalanced radiation force, thus breaking the positional balance. As a result, solutions to stably trap these objects are usually not found.

TABLE I. The retrieved transducer parameters and the dimensionless errors defined in Eq. (21). The radiation force and torque are evaluated using Eqs. (9) and (10). The gravity is $G \approx 422.4$ μN for all objects with an averaged radius of $a = 7$ mm and a density of $\rho_{\mathrm{p}} = 30$ kg/m^3.

	Sphere	Spheroid	Disk
A_i	$\begin{bmatrix} 0.30 & 0.30 & 0.31 & 0.30 & 0.30 \\ 0.30 & 2.39 & 2.16 & 2.39 & 0.30 \\ 0.31 & 2.16 & 0.16 & 2.16 & 0.31 \\ 0.30 & 2.39 & 2.16 & 2.39 & 0.30 \\ 0.30 & 0.30 & 0.31 & 0.30 & 0.30 \end{bmatrix}$	$\begin{bmatrix} 0.49 & 0.51 & 0.40 & 0.51 & 0.49 \\ 0.51 & 2.75 & 3.56 & 2.75 & 0.51 \\ 0.40 & 3.56 & 0.72 & 3.56 & 0.40 \\ 0.51 & 2.75 & 3.56 & 2.75 & 0.51 \\ 0.49 & 0.51 & 0.40 & 0.51 & 0.49 \end{bmatrix}$	$\begin{bmatrix} 2.46 & 2.40 & 2.37 & 2.40 & 2.46 \\ 2.40 & 1.38 & 0.28 & 1.38 & 2.40 \\ 2.37 & 0.28 & 0.03 & 0.28 & 2.37 \\ 2.40 & 1.38 & 0.28 & 1.38 & 2.40 \\ 2.46 & 2.40 & 2.37 & 2.40 & 2.46 \end{bmatrix}$
α_i [rad]	$\begin{bmatrix} -3.08 & 3.04 & 3.07 & 3.04 & -3.08 \\ 3.04 & -2.34 & -2.46 & -2.34 & 3.04 \\ 3.07 & -2.46 & 0.29 & -2.46 & 3.07 \\ 3.04 & -2.34 & -2.46 & -2.34 & 3.04 \\ -3.08 & 3.04 & 3.07 & 3.04 & -3.08 \end{bmatrix}$	$\begin{bmatrix} -3.09 & 3.05 & 3.06 & 3.05 & -3.09 \\ 3.05 & -2.37 & -2.08 & -2.37 & 3.05 \\ 3.06 & -2.08 & -1.16 & -2.08 & 3.06 \\ 3.05 & -2.37 & -2.08 & -2.37 & 3.05 \\ -3.09 & 3.05 & 3.06 & 3.05 & -3.09 \end{bmatrix}$	$\begin{bmatrix} -3.08 & 3.04 & 3.07 & 3.04 & -3.08 \\ 3.04 & -2.78 & -2.82 & -2.78 & 3.04 \\ 3.07 & -2.82 & 1.25 & -2.82 & 3.07 \\ 3.04 & -2.78 & -2.82 & -2.78 & 3.04 \\ -3.08 & 3.04 & 3.07 & 3.04 & -3.08 \end{bmatrix}$
$\vec{F}$ [μN]	$\begin{bmatrix} \approx 0 & \approx 0 & 418.6 \end{bmatrix}$	$\begin{bmatrix} \approx 0 & \approx 0 & 415.8 \end{bmatrix}$	$\begin{bmatrix} \approx 0 & \approx 0 & 431.4 \end{bmatrix}$
$\vec{T}$ [N $\cdot$ m]	$\begin{bmatrix} 7 & 3 & 3 \end{bmatrix} \times 10^{-22}$	$\begin{bmatrix} 4 & 3 & 5 \end{bmatrix} \times 10^{-19}$	$\begin{bmatrix} 4 & 3 & -5 \end{bmatrix} \times 10^{-20}$
$\mathrm{err}_{\mathrm{FT}}$	0.9 %	1.6 %	2.1 %

VIII. CONCLUSION AND DISCUSSION

This work theoretically demonstrates the ability to stably trap the macroscopic axisymmetric objects at a specific axial distance from the ultrasound transducer array. To achieve this, we obtain the acoustic scattered field around a non-spherical object with the help of the conformal transformation approach, and further formulate the radiation force and torque. The force and torque are then reconstructed and explicitly related to the transducer parameters, assembled into a system of nonlinear equations. Finally, the amplitude and phase patterns are obtained iteratively through the inverse solution of the nonlinear system to balance all the desired force and torque, while satisfying the constraints of Lyapunov stability conditions.

Specifically, we demonstrate that the macroscopic non-spherical objects with an averaged radius of $a = 7$ mm (or $ka \approx 5.18$) can be stably trapped at a specified axial height [for sphere, spheroid, and disk in Figs. 5, 6, and 7, respectively]. This indicates that we can apply higher-frequency waves to manipulate the non-spherical Mie objects rather than deliberately employing lower-frequency waves to impair the scattering contributions for the Rayleigh objects. Moreover, the desired radiation force and torque here are quasi-explicitly related to the transducer parameters through a system of nonlinear equations [Eq. (19)] instead of indirect control by implementing the gradient of the Gor'kov potential, which points the micro-objects to the destination locations of the potential wells [24, 26, 28].

It is worth mentioning that, throughout this paper, we assume the transducers as circular radiators [Eq. (1)], while the transducers could be extended to any kind of sound source by simply providing the desired velocity potential function to estimate the beam-shape coefficients in Eq. (6).

Note that the results discussed in this paper are under the premise that the symmetric axis of the levitated objects is consistent with the direction of wave propagation [or z-axis in Fig. 2]. With the help of the concept that the rotation of the object above the transducer array is mathematically equivalent to the inverse rotation of the array when the object is fixed [22], the proposed method could be extended to accommodate the cases that the axisymmetric objects are initially levitated in arbitrary orientations. While the pressure amplitude field [Eq. (1)], the relative position vector $\vec{r}^{(jq)}$, and the radiation force and torque [Eqs. (15) and (16)] should be properly rotationally transformed [according to Eqs. (4), (7), (25), and (26) in [22]].

ACKNOWLEDGMENTS

The first author acknowledges the support of the Ph.D. studentship from the University of Hong Kong.

Appendix A: EXPRESSIONS FOR THE STRUCTURE FUNCTIONS

The general structural functions $\mathbf{\Gamma}_n^{n',m'}$ and $\mathbf{\Lambda}_n^{n',m'}$, as functions of radial coordinate u, are given as [21, 22]

$$\begin{cases} \mathbf{\Gamma}_n^{n',m'} = \int_0^\pi j_n(kr)\, Q_n^m P_n^{m'}(\cos\theta)\, P_{n'}^{m'}(\cos w) \sin w \mathrm{d}w \\ \mathbf{\Lambda}_n^{n',m'} = \int_0^\pi h_n(kr)\, Q_n^m P_n^{m'}(\cos\theta)\, P_{n'}^{m'}(\cos w) \sin w \mathrm{d}w \end{cases}, \tag{A1}$$

where $P_{n'}^{m'}(\cdot)$ represents the associated Legendre function of n'-th order and m'-th degree for the variable therein, and $Q_n^m = \sqrt{\frac{(2n+1)}{4\pi} \cdot \frac{(n-m)!}{(n+m)!}}$. The physical coordinates r and θ are connected with the mapping coordinates u and w by

$$\begin{cases} r(u,w) = \sqrt{f(u,w)^2 + g(u,w)^2} \\ \theta(u,w) = \cos^{-1}\left(g(u,w)/r(u,w)\right) \end{cases}, \tag{A2}$$

and the mapping functions $g(u,w)$ and $f(u,w)$ are introduced to trigonometry prescribe of the body surface, in the physical space through the mapping coefficients c_n:

$$\begin{cases} g(u,w) = c_{-1}\mathrm{e}^{u}\cos(w) + \sum\limits_{n=0}^{\infty} c_n \mathrm{e}^{-nu}\cos(nw) \\ f(u,w) = c_{-1}\mathrm{e}^{u}\sin(w) - \sum\limits_{n=0}^{\infty} c_n \mathrm{e}^{-nu}\sin(nw) \end{cases}. \tag{A3}$$

In the mapping coordinate system, the object surface can be described as $u = u_0$. Hence, for the objects with Dirichlet boundary condition in Eq. (7), the structural functions $\Gamma_n^{n',m'}$ and $\Lambda_n^{n',m'}$ become

$$\begin{cases} \Gamma_n^{n',m'} = \boldsymbol{\Gamma}_n^{n',m'}\Big|_{u=u_0} \\ \Lambda_n^{n',m'} = \boldsymbol{\Lambda}_n^{n',m'}\Big|_{u=u_0} \end{cases}. \tag{A4}$$

Consistently, for the objects with Neumann boundary condition in Eq. (8), the partial derivatives of the structural functions in terms of u-direction are

$$\begin{cases} \Gamma_{n,u}^{n',m'} = \frac{\partial \boldsymbol{\Gamma}_n^{n',m'}}{\partial u}\Big|_{u=u_0} \\ \Lambda_{n,u}^{n',m'} = \frac{\partial \boldsymbol{\Lambda}_n^{n',m'}}{\partial u}\Big|_{u=u_0} \end{cases}. \tag{A5}$$

For different geometries, the mapping coefficients c_n are varied significantly. A method to solve the mapping coefficients c_n is provided in [41]. Generally, the mapping coefficients for typical sphere, spheroid, cone, diamond, and disk are, respectively, $c_n = [a, 0]$, $c_n = [a, 0, a/5]$, $c_n = [a, 0, 0, a/8]$, $c_n = [a, 0, 0, 0, a/10]$, and $c_n = [a, 0, -a/2, 0, -a/10, 0, -a/30]$ [21, 22], where a is the averaged radius used to proportionally stretch the size of the geometry. The first element in c_n describes the averaged radius, and the other elements capture the information of the non-spherical features.

Appendix B: EXPRESSIONS FOR THE COEFFICIENTS

The characteristic coefficients in terms of the i-th and j-th systems are calculated by:

$$
\begin{aligned}
M_{Fx}^{(ij)} &= \sum_{n,m} \Big(A_{n+1}^{m+1} R_{n,n+1}^{m,m+1(ij)} - B_{n-1}^{m+1} R_{n,n-1}^{m,m+1(ij)} \\
&\quad + C_{n+1}^{m-1} R_{n,n+1}^{m,m-1(ij)} - D_{n-1}^{m-1} R_{n,n-1}^{m,m-1(ij)} \Big), \\
N_{Fx}^{(ij)} &= \sum_{n,m} \Big(A_{n+1}^{m+1} I_{n,n+1}^{m,m+1(ij)} - B_{n-1}^{m+1} I_{n,n-1}^{m,m+1(ij)} \\
&\quad + C_{n+1}^{m-1} I_{n,n+1}^{m,m-1(ij)} - D_{n-1}^{m-1} I_{n,n-1}^{m,m-1(ij)} \Big), \\
M_{Fy}^{(ij)} &= \sum_{n,m} \Big(A_{n+1}^{m+1} R_{n,n+1}^{m,m+1(ij)} - B_{n-1}^{m+1} R_{n,n-1}^{m,m+1(ij)} \\
&\quad - C_{n+1}^{m-1} R_{n,n+1}^{m,m-1(ij)} + D_{n-1}^{m-1} R_{n,n-1}^{m,m-1(ij)} \Big), \\
N_{Fy}^{(ij)} &= \sum_{n,m} \Big(A_{n+1}^{m+1} I_{n,n+1}^{m,m+1(ij)} - B_{n-1}^{m+1} I_{n,n-1}^{m,m+1(ij)} \\
&\quad - C_{n+1}^{m-1} I_{n,n+1}^{m,m-1(ij)} + D_{n-1}^{m-1} I_{n,n-1}^{m,m-1(ij)} \Big), \\
M_{Fz}^{(ij)} &= \sum_{n,m} \Big(E_{n+1}^{m} R_{n,n+1}^{m,m(ij)} - F_{n-1}^{m} R_{n,n-1}^{m,m(ij)} \Big), \\
N_{Fz}^{(ij)} &= \sum_{n,m} \Big(E_{n+1}^{m} I_{n,n+1}^{m,m(ij)} - F_{n-1}^{m} I_{n,n-1}^{m,m(ij)} \Big), \\
M_{Tx}^{(ij)} &= \sum_{n,m} \Big(G_{n}^{m} R_{n,n}^{m,m+1(ij)} + G_{n}^{-m} R_{n,n}^{m,m-1(ij)} \Big), \\
N_{Tx}^{(ij)} &= \sum_{n,m} \Big(G_{n}^{m} I_{n,n}^{m,m+1(ij)} + G_{n}^{-m} I_{n,n}^{m,m-1(ij)} \Big), \\
M_{Ty}^{(ij)} &= \sum_{n,m} \Big(G_{n}^{m} R_{n,n}^{m,m+1(ij)} - G_{n}^{-m} R_{n,n}^{m,m-1(ij)} \Big), \\
N_{Ty}^{(ij)} &= \sum_{n,m} \Big(G_{n}^{m} I_{n,n}^{m,m+1(ij)} - G_{n}^{-m} I_{n,n}^{m,m-1(ij)} \Big), \\
M_{Tz}^{(ij)} &= \sum_{n,m} m R_{n,n}^{m,m(ij)}, \\
N_{Tz}^{(ij)} &= \sum_{n,m} m I_{n,n}^{m,m(ij)},
\end{aligned}
\tag{B1}
$$

where $R_{n,v}^{m,u(ij)}$ and $I_{n,v}^{m,u(ij)}$ are defined in Eq. (12), and the weighting coefficients are

$$
\begin{aligned}
A_n^m &= -C_n^{-m} = -\sqrt{\frac{(n+m-1)\,(n+m)}{(2n-1)\,(2n+1)}}, \\
B_n^m &= -D_n^{-m} = \sqrt{\frac{(n-m+2)\,(n-m+1)}{(2n+1)\,(2n+3)}}, \\
E_n^m &= F_{n-1}^m = \sqrt{\frac{(n-m)\,(n+m)}{(2n-1)\,(2n+1)}}, \\
G_n^m &= \sqrt{(n-m)\,(n+m+1)}.
\end{aligned}
\tag{B2}
$$

[1] P. J. Westervelt, The theory of steady forces caused by sound waves, The Journal of the Acoustical Society of America **23**, 312 (1951).
[2] P. J. Westervelt, Acoustic radiation pressure, The Journal of the Acoustical Society of America **29**, 26 (1957).
[3] G. Maidanik, Torques due to acoustical radiation pressure, The Journal of the Acoustical Society of America **30**, 620 (1958).
[4] L. Zhang and P. L. Marston, Angular momentum flux of nonparaxial acoustic vortex beams and torques on axisymmetric objects, Physical Review E **84**, 065601 (2011).
[5] A. A. Doinikov, Acoustic radiation pressure on a compressible sphere in a viscous fluid, Journal of Fluid Mechanics **267**, 1 (1994).
[6] A. A. Doinikov, Acoustic radiation force on a spherical particle in a viscous heat-conducting fluid. i. general formula, The Journal of the Acoustical Society of America **101**, 713 (1997).
[7] G. T. Silva, An expression for the radiation force exerted by an acoustic beam with arbitrary wavefront (l), The Journal of the Acoustical Society of America **130**, 3541 (2011).
[8] G. Silva, T. Lobo, and F. Mitri, Radiation torque produced by an arbitrary acoustic wave, EPL (Europhysics Letters) **97**, 54003 (2012).
[9] L. Zhang and P. L. Marston, Geometrical interpretation of negative radiation forces of acoustical bessel beams on spheres, Physical Review E **84**, 035601 (2011).
[10] F. Mitri, T. Lobo, and G. Silva, Axial acoustic radiation torque of a bessel vortex beam on spherical shells, Physical Review E **85**, 026602 (2012).
[11] J. H. Lopes, M. Azarpeyvand, and G. T. Silva, Acoustic interaction forces and torques acting on suspended spheres in an ideal fluid, IEEE transactions on ultrasonics, ferroelectrics, and frequency control **63**, 186 (2015).
[12] T. Tang and L. Huang, Mie particle assembly by a converging ultrasound field and acoustic interaction forces, Applied Acoustics **180**, 108123 (2021).
[13] T. Tang, B. Dong, and L. Huang, Agglomeration of particles by a converging ultrasound field and their quantitative assessments, Ultrasonics sonochemistry **75**, 105590 (2021).
[14] T. Tang and L. Huang, Acoustic radiation force for multiple particles over a wide size-scale by multiple ultrasound sources, Journal of Sound and Vibration **509**, 116256 (2021).
[15] F. Mitri, Axial acoustic radiation force on rigid oblate and prolate spheroids in bessel vortex beams of progressive, standing and quasi-standing waves, Ultrasonics **74**, 62 (2017).
[16] F. Mitri, Radiation force and torque on perfect electrically–conducting (pec) corrugated circular and elliptical cylinders in te or tm polarized plane progressive waves with arbitrary incidence, Journal of Quantitative Spectroscopy and Radiative Transfer **235**, 15 (2019).
[17] G. T. Silva and B. W. Drinkwater, Acoustic radiation force exerted on a small spheroidal rigid particle by a beam of arbitrary wavefront: Examples of traveling and standing plane waves, The Journal of the Acoustical Society of America **144**, EL453 (2018).
[18] Z. Gong, W. Li, F. G. Mitri, Y. Chai, and Y. Zhao, Arbitrary scattering of an acoustical bessel beam by a rigid spheroid with large aspect-ratio, Journal of Sound and Vibration **383**, 233 (2016).
[19] Z. Gong and M. Baudoin, Acoustic radiation torque on a particle in a fluid: An angular spectrum based compact expression, The Journal of the Acoustical Society of America **148**, 3131 (2020).
[20] D. B. Reeder and T. K. Stanton, Acoustic scattering by axisymmetric finite-length bodies: An extension of a two-dimensional conformal mapping method, The Journal of the Acoustical Society of America **116**, 729 (2004).
[21] T. Tang and L. Huang, An efficient semi-analytical procedure to calculate acoustic radiation force and torque for axisymmetric irregular bodies, Journal of Sound and Vibration **532**, 117012 (2022).
[22] T. Tang and L. Huang, Theoretical framework to predict the acoustophoresis of axisymmetric irregular objects above an ultrasound transducer array, Physical Review E **105**, 055110 (2022).
[23] B. W. Drinkwater, Dynamic-field devices for the ultrasonic manipulation of microparticles, Lab on a Chip **16**, 2360 (2016).
[24] A. Marzo and B. W. Drinkwater, Holographic acoustic tweezers, Proceedings of the National Academy of Sciences **116**, 84 (2019).
[25] R. Hirayama, D. Martinez Plasencia, N. Masuda, and S. Subramanian, A volumetric display for visual, tactile and audio presentation using acoustic trapping, Nature **575**, 320 (2019).
[26] A. Marzo, S. A. Seah, B. W. Drinkwater, D. R. Sahoo, B. Long, and S. Subramanian, Holographic acoustic elements for manipulation of levitated objects, Nature communications **6**, 1 (2015).
[27] S. D. Mellin and G. P. Nordin, Limits of scalar diffraction theory and an iterative angular spectrum algorithm for finite aperture diffractive optical element design, Optics Express **8**, 705 (2001).
[28] K. Melde, A. G. Mark, T. Qiu, and P. Fischer, Holograms for acoustics, Nature **537**, 518 (2016).
[29] T. Tang and L. Huang, Soundiation: A multi-functional gui-based software in evaluation of the acoustophoresis by the acoustic radiation force and torque on arbitrary axisymmetric objects, arXiv preprint arXiv:2202.04526 (2022).
[30] S. Inoue, S. Mogami, T. Ichiyama, A. Noda, Y. Makino, and H. Shinoda, Acoustical boundary hologram for macroscopic rigid-body levitation, The Journal of the Acoustical Society of America **145**, 328 (2019).
[31] G. T. Silva, B. A. L, L. J. Henrique, and M. F. G, Computing the acoustic radiation force exerted on a sphere using the translational addition theorem, IEEE transactions on ultrasonics, ferroelectrics, and frequency control **62**, 576 (2015).

[32] P. A. Martin, *Multiple scattering: interaction of time-harmonic waves with N obstacles*, 107 (Cambridge University Press, 2006).
[33] J. D. N. Cheeke, *Fundamentals and applications of ultrasonic waves* (CRC press, 2010).
[34] E. G. Williams, *Fourier acoustics: sound radiation and nearfield acoustical holography* (Academic press, 1999).
[35] A. P. Seyranian and A. A. Mailybaev, *Multiparameter stability theory with mechanical applications*, Vol. 13 (World Scientific, 2003).
[36] K. Levenberg, A method for the solution of certain non-linear problems in least squares, Quarterly of applied mathematics **2**, 164 (1944).
[37] D. W. Marquardt, An algorithm for least-squares estimation of nonlinear parameters, Journal of the society for Industrial and Applied Mathematics **11**, 431 (1963).
[38] G. T. Silva, Acoustic radiation force and torque on an absorbing compressible particle in an inviscid fluid, The Journal of the Acoustical Society of America **136**, 2405 (2014).
[39] J. Leão-Neto and G. T. Silva, Acoustic radiation force and torque exerted on a small viscoelastic particle in an ideal fluid, Ultrasonics **71**, 1 (2016).
[40] A. Marzo, A. Ghobrial, L. Cox, M. Caleap, A. Croxford, and B. Drinkwater, Realization of compact tractor beams using acoustic delay-lines, Applied Physics Letters **110**, 014102 (2017).
[41] D. T. DiPerna and T. K. Stanton, Sound scattering by cylinders of noncircular cross section: A conformal mapping approach, The Journal of the Acoustical Society of America **96**, 3064 (1994).